Rev. Adv. Mater. Sci. 38 (2014) 7-16

CLUSTER ION IMPLANTATION IN GRAPHITE AND DIAMOND: RADIATION DAMAGE AND STOPPING OF CLUSTER CONSTITUENTS

Vladimir N. Popok

Department of Physics and Nanotechnology, Aalborg University, 9220 Aalborg Øst, Denmark

Received: January 21, 2014

Abstract. Cluster ion beam technique is a versatile tool which can be used for controllable formation of nanosize objects as well as modification and processing of surfaces and shallow layers on an atomic scale. The current paper present an overview and analysis of data obtained on a few sets of graphite and diamond samples implanted by keV-energy size-selected cobalt and argon clusters. One of the emphases is put on pinning of metal clusters on graphite with a possibility of following selective etching of graphene layers. The other topic of concern is related to the development of scaling law for cluster implantation. Implantation of cobalt and argon clusters into two different allotropic forms of carbon, namely, graphite and diamond is analysed and compared in order to approach universal theory of cluster stopping in matter.

1. INTRODUCTION

Ion-beam treatment of materials is one of the widely applied techniques for numerous research and industrial purposes. Along with traditional monomers, atomic or molecular clusters (aggregates of atoms or molecules) have attracted considerable attention during the last two decades [1-4]. A cluster can be formed from atoms of the same chemical element or from two or more different species. Their sizes can vary from a few up to many thousands of constituents. Medium and large size clusters have diameters on the scale of nanometers. They are often called nanoparticles (NPs).

Clusters are used as models to investigate fundamental physical aspects of the transition from the atomic scale to bulk material [5]. Finite size effects in supported (deposited) NPs lead to specific properties which are of great interest for practical applications in areas such as electronics and optics, biology and medicine, catalysis and other nanotechnology-related branches [2,6,7-12]. Increase of cluster kinetic energy provides a possibility to tune the cluster-surface interaction regime towards implantation [4,13-17]. In this paper one of emphases is put on pinning of metal clusters on graphite surface with following etching of graphene layers. The interest in graphene comes from promises for a number of applications in nanoelectronics, plasmonics, sensing etc. See, for example [18,19] and references there in.

For developing successful applications of energetic clusters beams, a theory of cluster stopping in matter is required. Unfortunately, the existing theory for conventional ion implantation can be applied to cluster ions only for a very limited number of cases due to the fact that cluster is an aggregate of weakly bonded atoms or molecules providing multiple collision effect with a target. Therefore, the other emphasis of this paper is put on the development of scaling laws for cluster implantation.

Main materials under the discussion is graphite or highly ordered pyrolytic graphite (HOPG) and dia-

Corresponding author: Vladimir N. Popok, e-mail: vp@nano.aau.dk

mond. Graphite is chosen for modelling and experiments because it has an atomically smooth surface that makes it easy to resolve very small features on the sub-nm scale. Layered structure of graphite with covalent bonds in the graphene layers and van der Waals interactions between them is an interesting type of crystalline arrangement for modelling of cluster implantation. The data on implantation into graphite are compared with the results of cluster implantation into diamond, another allotropic form of carbon with strong and directional covalent bonds. This material is of significant practical interest. Some of its electronic characteristics, for instance, the high mobility of electrons and holes, low noise and leakage current as well as extremely high thermal conductivity make diamond attractive for high-power and high-frequency electronics [20]. Diamond is also considered as a potential platform of solid-state quantum devices.

2. CLUSTER BEAM IMPLANTATION AND EXPERIMENTAL METHODS

Cluster ion implantation was carried out using cluster implantation and deposition apparatus (CIDA) [21] with attached pulsed cluster source (PUCLUS) [22] and laser ablation cluster source (LACS) [23]. Argon clusters were produced by PUCLUS [24,25]. The mean sizes used in these experiments were 16, 27, and 41 atoms; the kinetic energy varied between 1.6 and 16 keV/cluster. LACS was used for the production of cobalt clusters with mean sizes of 30, 50, and 63 atoms accelerated to the energies between 0.25-10.1 keV/cluster [26]. All implantations were carried out at normal incidence to the sample surface in ultra-high vacuum (UHV) of ca. 10^{-9} Torr at room temperature.

Samples of HOPG had area of ca. 1 cm^2 and thickness of 1 mm. Surface of HOPG was cleaved with the help of adhesive tape prior the placement in the load-lock chamber, which was quickly evacuated to a vacuum of 10^{-7} Torr. After that the samples were moved into the implantation chamber. The cleaving and quick placement into vacuum were done to have fresh and clean surface. For the other series of experiments, small (with an area of a few mm^2) 1-mm thick plates of (111) synthetic diamond were used. No special treatment was applied to diamond surfaces prior the implantation.

Surfaces of the implanted samples were studied *ex situ* using a scanning probe laboratory Ntegra-Aura (NT-MDT). Atomic force microscopy (AFM) in a tapping mode and scanning tunnelling microscopy (STM) in the constant current mode were two main methods of measurements. Ultrasharp commercial cantilevers with curvature radius of tip 1-3 nm were utilized for AFM, while PtIr wires cut with the help of scissors were used for STM.

After the initial study by the above-mentioned methods the as-implanted samples were treated. HOPG was furnace annealed at 600 °C for 3-5 min. in ambient atmosphere. It is known that under such conditions presence of the defects (in this case caused by cluster impacts) in graphene layers leads to etching the damaged areas due to chemical reaction of carbon with atmospheric oxygen yielding volatile compounds. Etched areas typically have shape of hexagonal pits. Short-time annealing removes only the damaged volume down to the first underlying undamaged graphene plane [27-29]. Thus, measurement of depth of the pits provides information on the depth of radiation damage introduced by the cluster implantation.

Diamond was exposed to two stages of treatment. The first one was furnace annealing at 600 °C for 5-10 min in ambient atmosphere. The second one combined chemical processing with annealing. The samples were kept in 10% water solution of KNO_3 for 15 min., then heated up to 100 °C for 15 min. (to dry them) and finally annealed at 380 °C for 15 min. in ambient atmosphere to remove products of the chemical reaction. Both stages were intended to provide etching of radiation-damaged areas caused by individual cluster collisions. By measuring depth of the etched pits one can find the depth of radiation damage similar to the case of HOPG.

3. CLUSTER-SURFACE INTERACTION

Cluster-surface interaction can be divided into several regimes depending on the cluster kinetic energy: (i) soft landing, (ii) pinning and (iii) implantation [3].

The soft landing which is often called deposition of clusters is behind the subjects of the current paper and therefore does not discussed here. There is a number of publications studying properties of different supported clusters as well as reviewing these issues. See, for example, [6,7,9,30-33] and references there in.

If kinetic energy recalculated per atom is close to or slightly overcomes cohesive energy the cluster undergoes a plastic deformation, it can lose a few constituents but the most of atoms are still bonded to each other. At the same time, the energy transferred to the substrate atoms upon collision can already be high enough to displace one or a

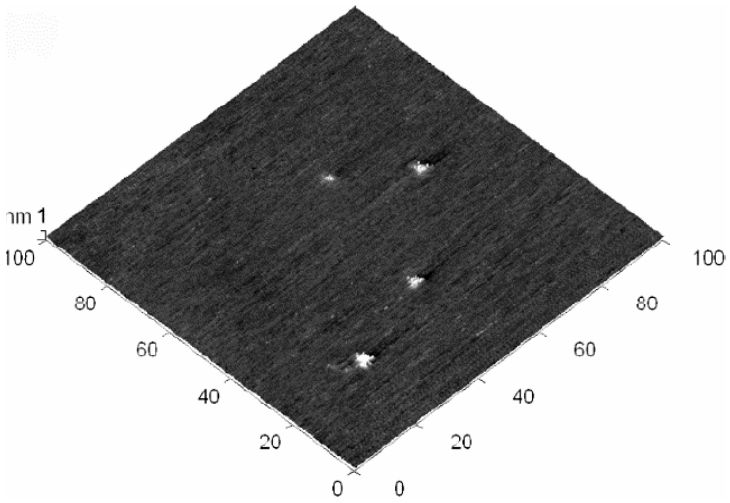

Fig. 1. STM image of HOPG surface after impact of Co_{50} clusters with energy of 350 eV/cluster (7 eV/atom).

few of them. Thus, some point defects are formed and the residual cluster becomes trapped at these sites, i.e. pinned [34]. Pinning is a boundary case between the soft landing and implantation of clusters. Pinning suppresses the cluster surface diffusion, thus, making advantages for a number of practical applications in which immobile particles on surface are required [10].

With further increase of kinetic energy the clusters are decomposed on impact and the constituents become implanted producing collision (radiation) defects in the matrix. Penetration depth of cluster constituents which is called projected range R_p as well as depth and mechanisms of radiation damage are functions of cluster energy and size. These questions are discussed below in more detail.

3.1. Pinning of Co_n clusters on graphite and etching of graphene layers

To obtain pinning of a small cluster, one can assume that only one carbon atom of the graphite target should be set into motion and this approach agrees rather well with the experiments, showing a linear dependence of E_{pin} (kinetic energy per atom corresponding to the pinning regime) on cluster size. In other words, the pinning energy per cluster constituent was found to be a constant value which varies between ca. 5 and 19 eV/atom from Ni to Au on impacts with HOPG [34-37]. One needs to mention, however, that the shape and structure of the pinned cluster is different from that prior the interaction with the surface. For instance, it was shown by MD simulations that medium-size gold clusters

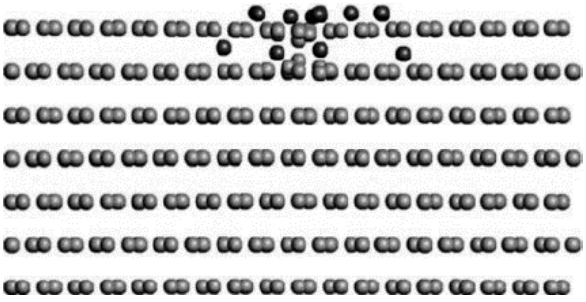

Fig. 2. MD simulation, viewed in cross section, of Co_{30} cluster 5 ps after the impact with energy of 300 eV/cluster (10 eV/atom) on graphite. Co atoms are shown in the darker shade. According to [26].

(which are nearly spherical before the impact) become rather spread out after the impact and can partially fragment while pinned nickel clusters are more compact but also far away from spherical or hemispherical shapes [38].

It was found in our experiments that size-selected Co_{50} clusters impacted HOPG with energies of 5-9 eV/atom (250-450 eV/cluster) formed surface bumps (Fig. 1) with mean diameters of ca. 1.5 nm and heights of ca. 0.3 nm [29]. Later experiments with Co_{30} and Co_{63} showed the same tendency on the surface bump formation [26]. MD simulations gave evidence that cobalt clusters of a few tens of atoms in size prefer to form single adatom layers on interaction with graphite while several cobalt atoms become embedded below the top graphene layer (Fig. 2) [26]. Thus, one can suggest that small bumps observed by STM and shown in Fig. 1 are Co islands formed by flattened on impact clusters and the energy regime of 5-9 eV/atom corresponds to pinning of cobalt clusters.

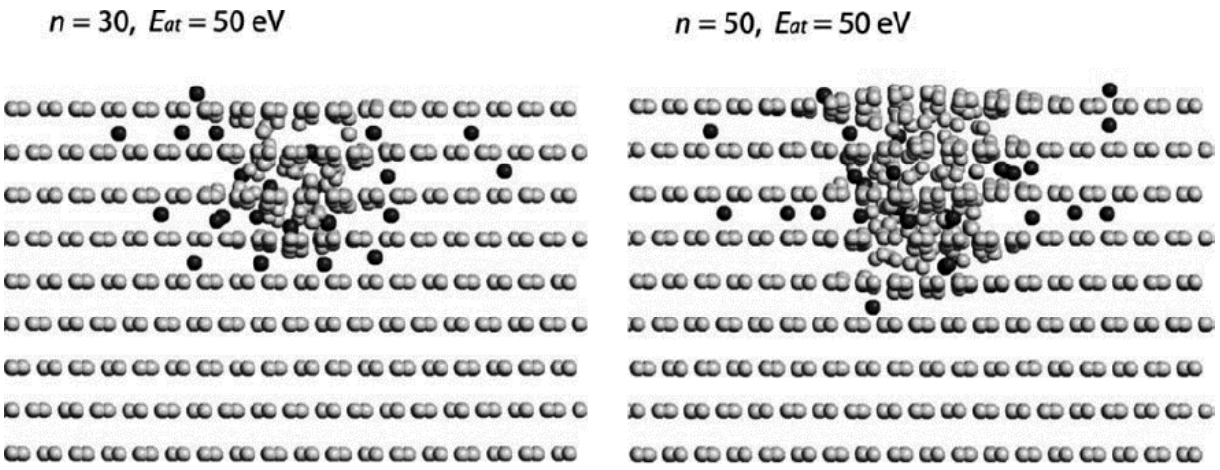

Fig. 3. MD simulations, viewed in cross section, of the damage created by impact of 50 eV/atom Co_{30} (left panel) and Co_{50} (right panel) clusters on graphite. Co atoms are shown in the darker shade. According to [26].

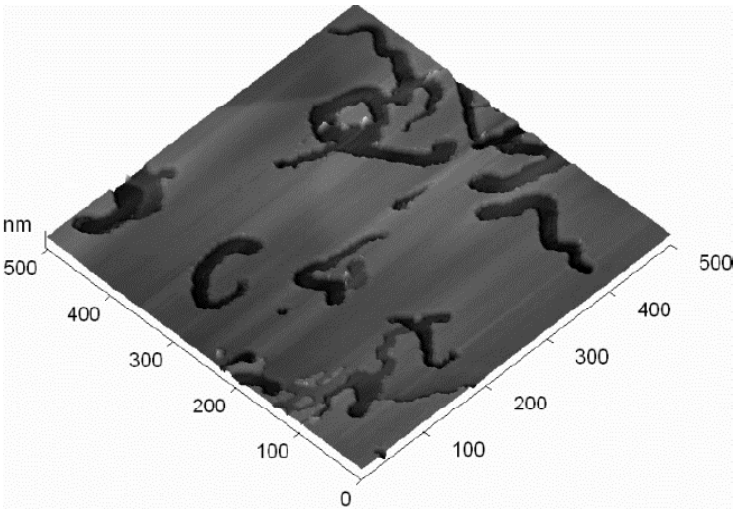

Fig. 4. STM image of the graphite surface after Co_{50} cluster impact with energy of 1500 eV/cluster (30 eV/atom) and following thermal-induced oxidative etching.

Interesting phenomenon was observed on these samples after the thermal annealing. For the case of Co_n clusters impacting HOPG with energies corresponding to the pinning threshold or slightly higher the formation of worm-like structures was found [29]. MD simulations predicted that for the energy around E_{pin} (ca. 5-9 eV/atom) the cluster introduces damage to very top graphene layer [39]. Depth of damage reaches 5 graphene layers if the energy is increased to ca. 50 eV/atom (Fig. 3) [26]. For the energies higher than E_{pin} the cluster is broken on impact but the constituents are implanted in close vicinity and their final location in HOPG is close to each other. One can assume that Co-Co bonds are restored to some extent, in other words, there is a residual cluster located in the shallow graphite layer. High temperature increases the diffusive mobility of these residual clusters and at the same time they catalyse the reaction of atmospheric oxygen with carbon, thus, favouring the formation of planar surface channels of random shape. For the impact energies around E_{pin} the depth of channels is 1 layer and they can be 200-300 nm long after a few minutes of the thermal treatment. For the higher energy the channels are deeper but the length is reduced to a few tens of nm as one can see in Fig. 4 for the case of 30 eV/atom Co_{50} clusters. Further energy increase leads to deep implantation and there are no surface channels produced by the thermal treatment; only pits. These cases are discussed below in Section 3.3.

Similar phenomenon of channel formation was reported elsewhere on the deposition of various chemical substances on graphite surfaces followed by heating [40]. The heating-induced etching was recently reported for Fe NPs deposited on few-layer

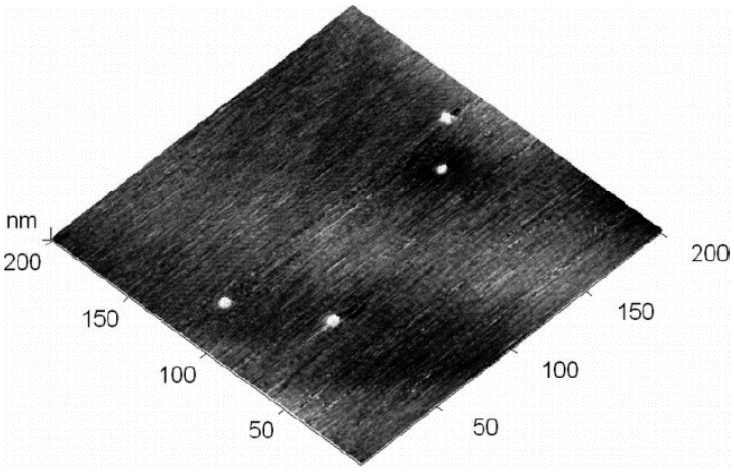

Fig. 5. STM image of HOPG surface implanted by Ar_{41} clusters with energy of 4.1 keV (100 eV/atom).

graphene [41]. While exposed to 900 °C, NPs etched away the graphene sheets producing channels. Trench channelling of graphene was also demonstrated by silver NPs under heating up to 650 °C in ambient atmosphere [42]. Trenching by NPs was suggested as a "catalytic pen" or prospect for high-precision lithography on graphenes.

3.2. Crater formation on HOPG and diamond

Energetic cluster colliding the surface can lead to crater formation. This phenomenon was extensively studied both experimentally and theoretically [43-52] and good understanding of the main effects governing the phenomenon was reached. It was found that substrate material plays an important role. Graphite is an allotropic form of carbon having layered structure with strong covalent bonds in graphene plains and week van der Waals interactions between the layers. Therefore, the graphite structure responds very elastically to cluster impact: the collision induces oscillations of the graphene planes [53]. For the case of Ar_{16} and Ar_{41} with energies up to 16 keV/cluster, the oscillations have very little influence on the structure outside the immediate impact region with primary displacement cascades. It was predicted by MD simulations that a crater can be formed only at the initial stage of impact [39]. The elastic behaviour of graphene sheets at a later stage causes efficient closure of the craters and only disordered areas are finally formed. These damaged areas were found by STM as tiny bumps (Fig. 5). It is worth noting that craters can be formed on HOPG but the clusters should be larger and they should have high kinetic energies in order to be able to provide high energy density transfer to the graphite target and local sputtering. One of such examples can be found in [54].

Higher density, melting (or sublimation) point and larger atomic displacement energies provide less favourable conditions for crater formation. Diamond is a good example of such material on which it is difficult to produce craters due to relatively high threshold energy needed to displace a carbon atom [25,53,55]. MD simulations showed no indication for molten diamond under the impact of Ar_{27} with energies up to 21 keV/cluster [53]. Thus, there is a low probability for crater formation through the mechanism involving compression, local melting and following liquid flow as often the case in other materials [56]. The cluster bombardment of diamond can cause craters only through direct sputtering of the surface atoms. Experimentally, a few craters with diameters of 5-7 nm are found using AFM (see Fig. 6) on the samples bombarded by argon clusters with energies $\geq$ of 12 keV/cluster ($\geq$ 440 eV/atom). In some cases small hillocks with height of 0.5-2.0 nm and basal diameter of 10-15 nm were observed which could be unresolved (due to tip convolution effect) craters.

3.3. Stopping of clusters in HOPG and diamond

It is mentioned in Section 2 that cluster ion implantation in HOPG followed by heat treatment in the presence of oxygen leads to the formation of pits with the depth corresponding to the depth of the radiation damage developed by the projectiles. To etch away the radiation damaged areas in diamond more complex procedure which is also described in Section 2 is applied. Examples of etched pits for both materials are shown in Fig. 7. Hexagonal shape

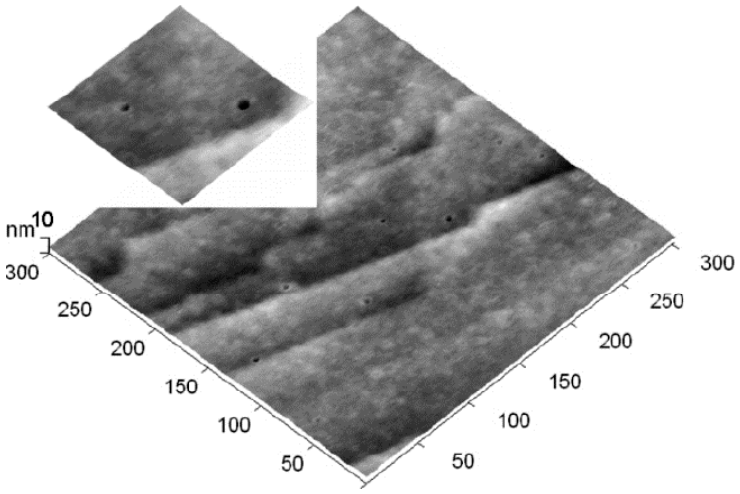

Fig. 6. AFM image of diamond surface implanted by Ar_{27}^{+} cluster ions with energy of 12 keV/cluster.

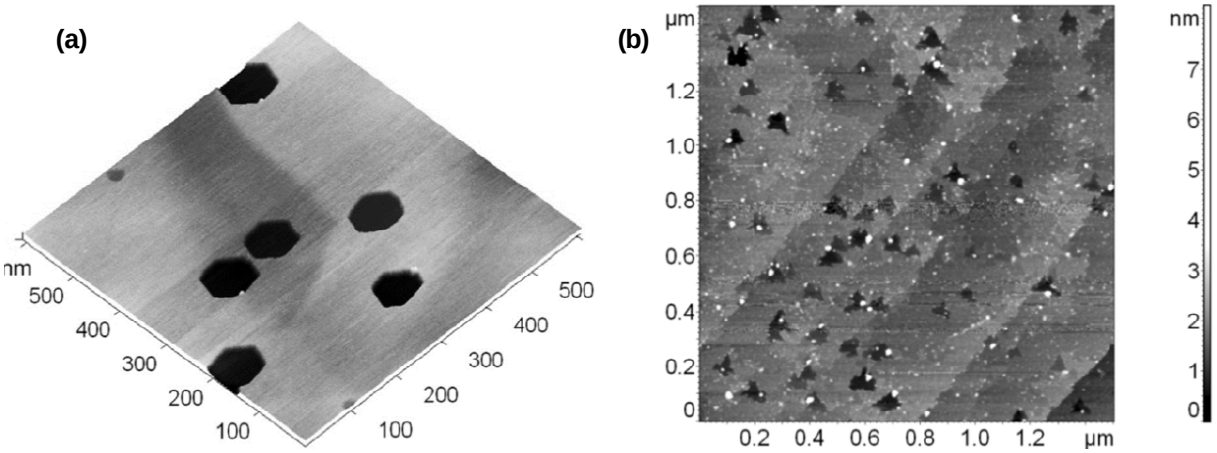

Fig. 7. AFM images of (a) HOPG surface implanted by Ar_{16}^{+} cluster ions with energy of 3.2 keV/cluster (200 eV/atom) and (b) diamond surface implanted by Ar_{27}^{+} cluster ions with energy 15 keV/cluster (ca. 560 eV/atom). Both samples underwent post-implantation treatments as described in the text. Pits in both images correspond to etched radiation damaged areas formed by cluster impacts.

for HOPG is related to its honey-comb structure while triangular shape for the diamond samples is caused by (111) crystallographic orientation.

AFM and STM are applied to measure depth of the pits in the implanted and annealed HOPG samples. It is known from MD simulations that mean projected range of cluster constituents is very close to the depth of radiation damage for relatively low keV-energies as in our case [24]. Thus, one can conclude that from the depth of the pits R_p can be extracted.

The measurements show that R_p of argon cluster constituents follows the square root of energy $E^{1/2}$ dependence in both HOPG and diamond (Fig. 8) [24,25]. Since cluster momentum $p \sim E^{1/2}$, it is suggested to scale R_p with momentum that leads to the linear scaling law shown in Fig. 9. The use of momentum allows considering the cluster size

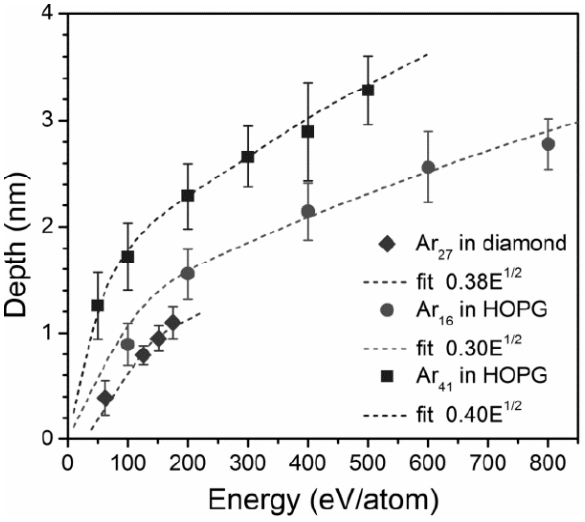

Fig. 8. Dependences of depth of radiation damage (or R_p) on energy and size of argon clusters implanted into HOPG and diamond.

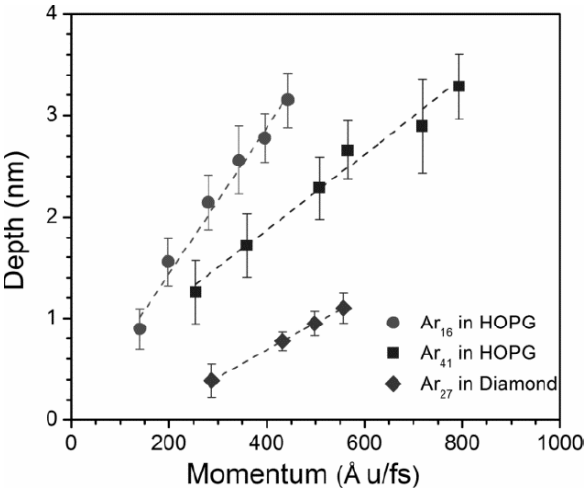

Fig. 9. Dependence of depth of radiation damage (or R_p) on momentum and size of argon clusters implanted into HOPG and diamond.

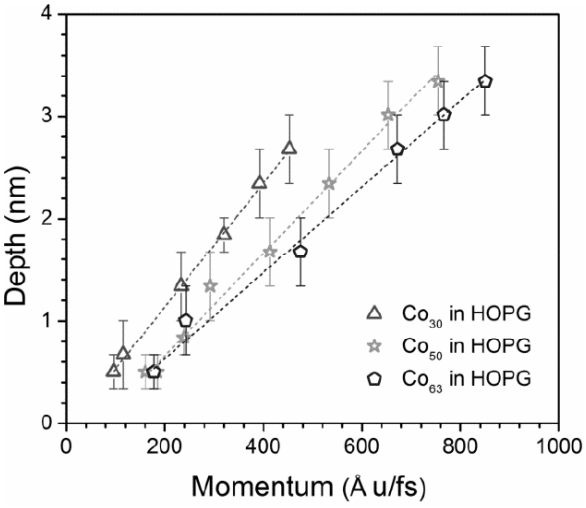

Fig. 10. Dependence of depth of radiation damage (or R_p) on momentum and size of cobalt clusters implanted into HOPG.

(through its mass) together with the energy, thus, using only one physical quantity. It can also be seen from the presented data that larger clusters with the same energy per atom are implanted deeper compared to the smaller ones. This phenomenon was earlier known as “clearing the way effect” [57,58]. In the current contents one can simply conclude that not energy but momentum is the important parameter to consider cluster stopping in matter and, therefore, the clusters with higher momentum are implanted deeper.

As one can see in Fig. 9, the linear fits for different sizes of argon clusters have different slopes. Similar dependences are observed for cobalt clusters (Fig. 10). This discrepancy can be removed by considering one more important parameter: an area of cluster-matter interaction. It can be found as a

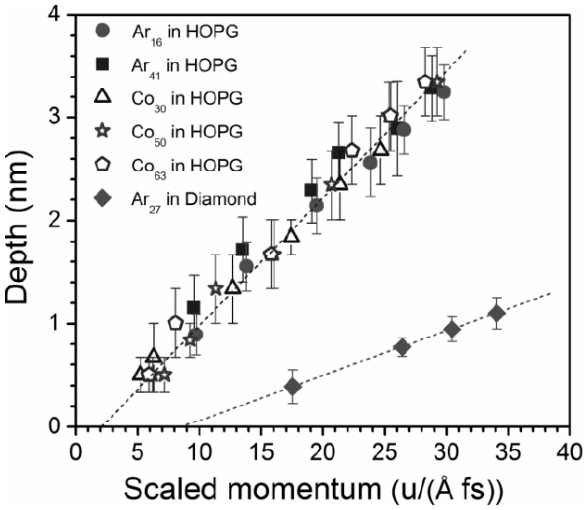

Fig. 11. Dependence of depth of radiation damage (or R_p) on scaled momentum and size of argon and cobalt clusters implanted into HOPG and diamond.

cross-sectional area of the cluster projected on the surface. Dividing the cluster momentum by this area, allows to introduce a scaled momentum suggested in [59]. Then, the data for different cluster sizes and different cluster species implanted in HOPG fall on the same fit straight line vs scaled cluster momentum as shown in Fig. 11. This provides very strong support of a universal scaling law for cluster stopping in matter with linear dependence on cluster momentum.

The data for diamond are also fitted with a straight line in the above-mentioned co-ordinates but this line has different tilt (see Fig. 11). This is related to the difference in threshold penetration energy and cluster stopping power for different types of target materials. For graphite, the energy of a few eV/atom is sufficient to make a radiation defect, i.e. to displace carbon atoms from its site. This conclusion follows from the pinning experiments. For diamond, such threshold energy is higher. As one can see in Fig. 8, the best-fit line for diamond crosses the energy axis at 35 eV. This value is close to 33 eV reported as minimal energy required for cluster sputtering of diamond [53]. Thus, to enter into diamond a cluster requires higher energy and higher momentum compared to graphite. To penetrate deeper a cluster also needs higher power due to the stronger bonds in diamond compared to graphite. Therefore, the fit line for diamond has higher offset for the intersection with *x* axis and lower tilt angle compared to that for HOPG as shown in Fig. 11.

It is worth mentioning that correct estimation of the cluster cross-section is an important point. For metal clusters a spherical cluster approximation

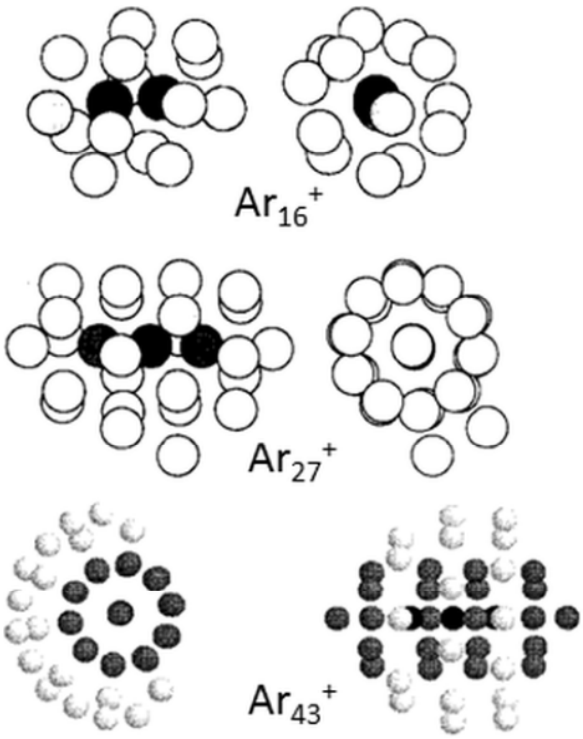

Fig. 12. Most stable geometries (front and side views) for charged argon clusters of particular sizes. The atoms carrying the charge in the core are shown in the dark shade. For Ar_{43}^+, grey shaded shell around the core represents highly-polarised atoms. According to [61,62].

works pretty well. It does not, however, provide a suitable approach for small rare gas clusters (Ar in our case) because the charge changes the geometrical packing of atoms in the cluster. It was suggested by Haberland and co-workers [60] that in argon cluster ions with $n \geq 6$, the charge is distributed among 4 core atoms. This ion core is surrounded by rings or "crowns" of adatoms. Theoretical calculations showed that the bond length shrinks to ca. 2.45-2.99 Å in the ion core compared to 3.76 Å in a neutral case [61,62]. The atoms surrounding the charged core become polarized thus providing an additional attractive interaction reducing the bond length and distorting the shape of the cluster. This effect of charge on the cluster packing was also confirmed experimentally [63]. In simulations, Ar_{16}^+ and Ar_{27}^+ cluster ions are predicted to be slightly elongated along the charged core (see Fig. 12) [61]. These geometries are considered for our calculations of the projected areas. In the case of Ar_{41}^+ cluster ion used in the experiments, the lowest energy geometry suggested for Ar_{43}^+ cluster ion in [62] (also see Fig. 12) is used for the calculations. In all three cases the cluster shapes could be quite well approximated by ellipsoids. The mean cross-section values are found applying the orientations of the impacting cluster giving the smallest and the largest projected areas on the surface. *Only* through the consideration of "compressed" argon clusters with the ellipsoid-like shape it has been possible to calculate the scaled momenta which were fitted by one line shown in Fig. 11.

5. CONCLUSIONS

HOPG and diamond samples implanted by keV energy size-selected cluster ions of argon and cobalt are studied using AFM and STM. There is a number of important conclusions that can be made from the obtained results.

It is found that cobalt clusters with energies between 5-9 eV/atom can be pinned to graphite surface. Clusters with slightly higher energies up to ca. 30-50 eV/atom are shallow implanted. The implanted cluster constituents are found to be located is close vicinity to each other. One can assume that Co-Co bonds are restored to some extent, in other words, there is a residual cluster in the shallow graphite layer. For the above-mentioned cluster energies, post-implantation annealing at ca. 600 °C for 5 min. leads to the formation of planar surface channels of random shape: high temperature increases the diffusive mobility of the residual clusters and at the same time they catalyse the reaction of atmospheric oxygen with carbon. This method can be suggested a "catalytic pen" or "scissors" to process lithography or selective etching of graphene.

Energetic cluster impact typically leads to the crater formation on the surface. On HOPG, clusters with energies higher than the pinning one can produce a radiation damage. However, for the case of graphite it is found that a crater can be formed only at the initial stage of impact. Elastic behaviour of graphene plains leads to efficient enclosure of the crater, thus, only small disordered area is formed. On diamond, higher energy is required to displace a carbon atom from its site which is found to be around 35 eV on cluster impact. The cluster bombardment can cause craters only through direct sputtering of the surface atoms because there is no molten phase for diamond. Experimentally, craters with diameters of 5-7 nm are found on the samples bombarded by argon clusters with energies ≥12 keV/cluster.

The implantation of argon clusters shows strong similarity to the implantation behaviour of cobalt clusters and demonstrates the universality of a simple empirical scaling law for cluster implantation into graphite. The found linear dependence of cluster stopping on momentum is completely different com-

pared to the stopping of monoatomic projectiles which linearly scales with energy. On the other hand, the proposed scaling law for cluster stopping creates a bridge to surface collisions of macroscopic bodies having their penetration depths linearly scaled with velocity. In the frameworks of this scaling law one can also easy explain deeper implantation of larger clusters compared to smaller ones at the same energy per cluster constituent. The stopping should be scaled not with energy but with momentum, thus, larger clusters yield higher momentum, i.e. lower stopping power and as a consequence a higher projected range.

Another important point to concern is area of cluster-surface interaction which can be assumed to be a cross-section of an impacting cluster projected on the surface. By considering this area a so-called scaled momentum is found and projected ranges for different cluster species implanted into HOPG with various sizes and energies can be put on the same best-fit line thus providing a strong support of the suggested scaling law. It is worth stressing that correct estimation of the cluster cross-section, which depends on the charge state and geometrical packing of atoms, is important.

For the argon cluster implantation into diamond very similar linear dependence of the implantation depth on scaled cluster momentum is found. However, the best-fit line is different from that for HOPG due to the high penetration threshold energy, which is found to be around 35 eV, and stopping powers in diamond.

REFERENCES

[1] P. Milani and S. Iannotta, *Cluster Beam Synthesis of Nanostructured Materials* (Springer, Berlin, 1999).

[2] *Metal Clusters at Surfaces*, ed. by K.-H. Meiwes-Broer (Springer, Berlin, 2000).

[3] V.N. Popok and E.E.B. Campbell // *Rev. Adv. Mater. Sci.* **36** (2006) 19.

[4] N. Toyoda and I. Yamada // *IEEE Trans. Plasma Sci.* **36** (2008) 1471.

[5] P. Jena and A.W. Castkeman Jr. // *Proc. Nation. Acad. Sci.* **103** (2006) 10560.

[6] C. Binns // *Surf. Sci. Rep.* **44** (2001) 1.

[7] K. Wegner, P. Piseri, H.V. Tafreshi and P. Milani // *J. Phys. D* **39** (2006) R439.

[8] U. Kreibig and M. Vollmer, *Optical Properties of Metal Clusters* (Springer, Berlin, 1995).

[9] A. Perez, P. Melinon, V. Dupius, P. Jensen, B. Prevel, J. Tuaillon, L. Bardotti, C. Marlet, M. Treilleux, M. Broyer, M. Pellarin, J.L. Vaille, B. Palpant and J. Lerme // *J. Phys. D: Appl. Phys.* **30** (1997) 709.

[10] R.E. Palmer, S. Pratontep and H.-G. Boyen // *Nature Mater.* **2** (2003) 443.

[11] *Atomic Clusters: From Gas Phase to Deposition*, ed. by D.P. Woodruff (Elsevier, Amsterdam, 2007).

[12] W.E. Kaden, T. Wu, W.A. Kunkel and S.L. Andersen // *Science* **326** (2009) 826.

[13] V. Popok, In: *Handbook of Nanophysics: Clusters and Fullerenes*, ed. by K.D. Sattler (CRC Press, Boca Raton, 2010), p. 19-1.

[14] V.N. Popok // *Mater. Sci. Eng. R: Rep.* **72** (2011) 137.

[15] V.N. Popok, I. Barke, E.E.B. Campbell and K.-H. Meiwes-Broer // *Surf. Sci. Rep.* **66** (2011) 347.

[16] J. Gspann, In: *Large Clusters of Atoms and Molecules*, ed. by T.P. Martin (Kluwer, Amsterdam, 1997), p. 443.

[17] I. Yamada, J. Matsuo, N. Toyoda and A. Kirkpatrick // *Mater. Sci. Eng. R: Rep.* **34** (2001) 231.

[18] C.N.R. Rao, A.K. Sood, R. Voggu and K.S. Subrahmanyam // *J. Phys. Chem. Lett.* **1** (2010) 572.

[19] W. Lu, P. Soukiassian and J. Boeckl // *MRS Bulletin* **37** (2012) 1119.

[20] C. Raynaud, D. Tournier, H. Morel and D. Planson // *Diamond Rel. Mater*. **19** (2010) 1.

[21] V.N. Popok, V.S. Prasalovich, M. Samuelsson and E.E.B. Campbell // *Rev. Sci. Instrum.* **73** (2002) 4283.

[22] V.N. Popok, V.S. Prasalovich and E.E.B. Campbell // *Nucl. Instrum. Meth. Phys. Res. B* **207** (2003) 145.

[23] S. Vučković, M. Svanqvist and V.N. Popok // *Rev. Sci. Instrum.* **79** (2008) 073303.

[24] V.N. Popok, J. Samela, K. Nordlund and E.E.B. Campbell // *Phys. Rev. B* **82** (2010) 201403(R).

[25] V.N. Popok, J. Samela, K. Nordlund and V.P. Popov // *Phys. Rev. B* **85** (2012) 033405.

[26] V.N. Popok, S. Vučković, J. Samela, T. Järvi, K. Nordlund and E.E.B. Campbell // *Phys. Rev. B* **80** (2009) 205419.

[27] G. Bräuchle, S. Richard-Schneider, D. Illig, J. Rockenberger, R.D. Beck and M.M. Kappes // *Appl. Phys. Lett.* **67** (1995) 52.

[28] Y. Yamamura and T. Muramoto // *Rad. Eff. Def. Sol.* **130-131** (1994) 225.

[29] S. Vučković, J. Samela, K. Nordlund and V.N. Popok // *Eur. Phys. J. D* **52** (2009) 107.

[30] R. Guerra, U. Tartaglino, A. Vanossi and E. Tosatti // *Nature Mater.* **9** (2010) 634.
[31] D. Fink, M. Muller, R. Klett, L.T. Chadderton, L. Palmetshofer, J. Kastner, J. Vacik, V. Hnatowicz and V. Popok // *Nucl. Instrum. Meth. Phys. Res. B* **103** (1995) 415.
[32] B. Yoon, V.M. Akulin, P. Cahuzac, F. Carlier, M. de Frutos, A. Masson, C. Mory, C. Colliex and C. Brechignac // *Surf. Sci.* **443** (1999) 76.
[33] P. Jensen // *Rev. Mod. Phys.* **71** (1999) 1695.
[34] S.J. Carroll, P. Weibel, B. von Issendorf, L. Kuipers and R.E. Palmer // *J. Phys.: Condens. Mater.* **8** (1996) L617.
[35] M. Di Vece, S. Palomba and R. E. Palmer // *Phys. Rev. B* **72** (2005) 73407.
[36] S. Gibilisco, M. Di Vece, S. Palomba, G. Faraci and R. E. Palmer // *J. Chem. Phys.* **125** (2006) 84704.
[37] R. Smith, C. Nock, S.D. Kenny, J.J. Belbruno, M. Di Vece, S. Palomba and R.E. Palmer // *Phys. Rev. B* **73** (2006) 125429.
[38] R. Smith, S.D. Kenny, J.J. Belbruno, R.E. Palmer, In: *The Chemical Physics of Solid Surfaces*, ed. by D.P. Woodruff (Elsevier, Amsterdam, 2007), p. 589.
[39] J. Samela, K. Nordlund, J. Keinonen, V.N. Popok and E.E.B. Campbell // *Eur. Phys. J. D* **43** (2007) 181.
[40] H. Chang and A. Bard // *J. Am. Chem. Soc.* **113** (1991) 558.
[41] S.S. Datta, D.R. Strachan, S.M. Khamis and A.T.C. Johnson // *Nano Lett.* **8** (2008) 1912.
[42] N. Severin, S. Kirstein, I.M. Sokolov and J.P. Rabe // *Nano Lett.* **9** (2009) 457.
[43] N. Toyoda, H. Kitani, N. Hagiwara, T. Aoki, J. Matsuo and I. Yamada // *Mater. Chem. Phys.* **54** (1998) 262.
[44] P. Webb, M. Kerford, M. Kappes and G. Brauchle // *Nucl. Instrum. Meth. Phys. Res. B* **122** (1997) 318.
[45] L.P. Allen, Z. Insepov, D.B. Fenner, C. Santeufemio, W. Brooks, K.S. Jones and I. Yamada // *J. Appl. Phys.* **92** (2002) 3671.
[46] V.N. Popok, S.V. Prasalovich and E.E.B. Campbell // *Vacuum* **76** (2004) 265.
[47] V.N. Popok, S.V. Prasalovich and E.E.B. Campbell // *Surf. Sci.* **566-568** (2004) 1179.
[48] S.V. Prasalovich, V.N. Popok, P. Persson, E.E.B. Campbell // *Eur. Phys. J. D* **36** (2005) 229.
[49] J. Samela, K. Nordlund, V.N. Popok and E.E.B. Campbell // *Phys. Rev. B* **77** (2008) 075309.
[50] V.N. Popok, J. Jensen, S. Vučković, A. Mackova and C. Trautmann // *J. Phys. D: Appl. Phys.* **42** (2009) 205303.
[51] Y. Yamaguchi and J. Gspann // *Phys. Rev. B* **66** (2002) 155408.
[52] K. Nordlund and J. Samela // *Nucl. Instrum. Meth. Phys. Res. B* **267** (2009) 1420.
[53] V.N. Popok, J. Samela, K. Nordlund and V.P. Popov // *Nucl. Instrum. Meth. Phys. Res. B* **282** (2012) 112.
[54] S. Houzumi, K. Mochiji, N. Toyoda and I. Yamada // *Jpn. J. Appl. Phys.* **44** (2005) 6252.
[55] J.F. Prins, T.E. Derry and J.P.F. Sellschop // *Phys. Rev. B* **34** (1986) 8870.
[56] K. Nordlund, T.T. Järvi, K. Meinander and J. Samela // *Appl. Phys. A* **91** (2008) 561.
[57] Y. Yamamura // *Nucl. Instrum. Meth. Phys. Res. B* **33** (1988) 493.
[58] V.I. Shulga and P. Sigmund // *Nucl. Instrum. Meth. Phys. Res. B* **47** (1990) 236.
[59] L. Seminara, P. Convers, R. Monot and W. Harbich // *Eur. Phys. J. D* **29** (2004) 49.
[60] H. Haberland, B. von Issendorf, T. Kolar, H. Kornmeier, C. Ludewigt and A. Rish // *Phys. Rev. Lett.* **67** (1991) 3290.
[61] N.L. Doltsinis, P.J. Knowles and F.Y. Naumkin // *Mol. Phys.* **96** (1999) 749.
[62] J.A. Gascón and R.W. Hall // *J. Phys. Chem. B* **105** (2001) 6579.
[63] S.V. Prasalovich, K. Hansen, M. Kjellberg, V.N. Popok and E.E.B. Campbell // *J. Chem. Phys.* **123** (2005) 084317.